www.adeepakpublishing.com

Krejci, D. et al. (2019): JoSS, Vol. 8, No. 2, pp. 881–893
(Peer-reviewed article available at www.jossonline.com)

www. JoSSonline.com

Full Performance Mapping of the IFM Nano Thruster, Including Direct Thrust Measurements

David Krejci, Valentin Hugonnaud, Tony Schönherr, Bryan Little, and Alexander Reissner
ENPULSION
Wiener Neustadt, Austria

Bernhard Seifert
FOTEC
Wiener Neustadt, Austria

Quirin Koch, Eduard Bosch Borràs, and José González del Amo
ESA-ESTEC
Noordwijk, Netherlands

Abstract

The IFM Nano Thruster is a Field Emission Electric Propulsion (FEEP) system using Indium as propellant. The core element of this propulsion technology is a passively fed, porous ion emitter consisting of 28 sharp emitter tips. Using differential biasing of the emitter and extractor electrodes, the IFM Nano Thruster can operate over a wide range of specific impulse from 2000 to 6000 s and beyond. At a total input power of 40 *W*, including heater for propellant liquefaction and neutralization to maintain neutral spacecraft potential, the IFM Nano Thruster can provide up to 350 µN. This work presents a test campaign conducted at the ESA Propulsion Laboratory (EPL), located at ESA ESTEC. Direct thrust measurements obtained on two thrusters are compared to analytical thrust models. Full performance envelope mapping, including direct thrust measurements, were performed for both thrusters, and a comparison to modelled performance envelope is presented herein, including a discussion of the major emitter parameters concerning their impact on the performance envelope.

1. Introduction

As the maturity and utility of small spacecraft platforms and missions increases, the number of missions including propulsion systems increases, enabling more complex missions, such as significant orbit transfer from the deployment orbit, constellation maintenance, formation flight, and deorbiting (Krejci, 2018; Lemmer, 2017; Selva, 2012). In addition, propulsive capabilities can be used for mission extension in low-Earth orbit (LEO) and high-total-impulse propulsion can enable interplanetary missions (Spangelo, 2015). Envisioned mission applications include high-temporal-resolution Earth observation and telecommunication network applications. The liquid metal

Corresponding Author: David Krejci – krejci@enpulsion.com
Publication History: Submitted – 12/24/18; Revision Accepted – 06/28/19; Published – 10/10/19

IFM Nano Thruster has been developed to address such mission needs (Vasiljevic et al., 2011; Jelem et al., 2017), allowing for high specific impulse due to the electrostatic acceleration principle (Tajmar, 2004) and high total impulse due to the high density of the propellant. Liquid metal indium sources have been developed for over 25 years at FOTEC and at the Austrian Institute of Technology, and have gained considerable space heritage (Fehringer, 1997; Tajmar, 2009). Based on this technology, liquid metal FEEP emitters for propulsive applications have been developed (Tajmar, 2010) and extensively tested, resulting in a multi-emitter design shown in Figure 1 during emission. The first IFM Nano Thruster based on this emitter technology has been successfully validated in space in 2018 (Seifert, 2018; Krejci, 2018).

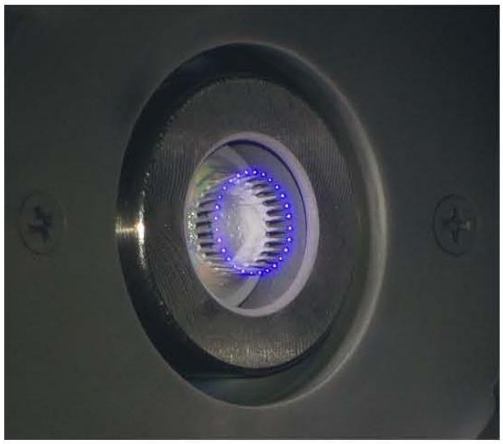

Figure 1. Close-up of IFM Nano Thruster during ion emission.

2. The IFM Nano Thruster

2.1. Operating Principle

Field Emission Electric Propulsion (FEEP) is based on extraction and ionization of propellant from a liquid metal, a process that can occur at field strengths in the order of 1 $V{\cdot}nm^{-1}$. To achieve the necessary local field strength, the liquid metal is usually suspended over a sharp emitter structure in needle form. Different configurations for passive propellant transport by capillary forces have been investigated, including capillary geometries, externally wetted needles, and porous needle-like structures. Electrostatic stressing of the liquid metal above a certain threshold causes the metal to deform into a Taylor cone (Taylor, 1964), further increasing the local field strength at the apex of the cone, where particle extraction is eventually achieved. In a FEEP device, the electrostatic potential is applied between the metal emitter (composed of the 28 porous needles placed in a crown-like shape) and a counter electrode called an extractor, which is designed to maximize transparency for emitted ions. The extractor, which is insulated from the emitter and thruster structure, surrounds the latter so that the electric field created by the potential difference is uniform all over the needle tips. Both voltage reference to the power processing unit, and therefore, electrical spacecraft ground, which also serves as ground for the neutralizer. The negative potential of the extractor can be actively controlled. In such a geometry, ions are then accelerated by the same electric field used for extraction and ionization, making this process highly efficient. The ion emission current extracted from the propellant suspended over the emitter needles is only dependent on the total discharge voltage, that is the potential difference between emitter and extractor potential. By controlling voltages of both the emitter and the extractor independently, the emission current can be controlled independently of the emitter potential, and hence the specific impulse. This allows operating the thruster in an envelope of specific impulse and thrust.

In addition to ions, instabilities in the Taylor cone and the jet (Mair, 1996; Tajmar, 2005) lead to additional expulsion of droplets, which do not contribute to the thrust, but lead to a net increase in the average propellant mass flow, therefore decreasing the specific impulse achieved (Tajmar, 2009).

Since a FEEP emitter expels positively charged ions, with electrons tunneling back into the metal propellant and therefore remaining within the thruster system, an additional means for electron emission is necessary to avoid charging of the thruster, and hence the entire spacecraft. A variety of different electron emitters are available, including thermionic neutralizers and electron emitters based on carbon nanotube forests (Tajmar, 2002). In the IFM Nano Thruster, thermionic neutralizers are used, in which a high

temperature filament is negatively biased with respect to the thruster ground. In this configuration, typically 3 to 5 *W* are used for filament heating and an additional maximum 1*W* in beam bias power.

2.2. The IFM Nano Thruster

The IFM Nano Thruster, shown in Figure 2, is a compact packaging of the heritage ion emitter, propellant reservoir, neutralizer, and power processing unit in a Cubesat-sized form factor approximately 80 *mm* in height. In addition to the centrally located ion emitter, two cold redundant neutralizers that are used to avoid spacecraft potential buildup are used in each IFM Nano Thruster. The thruster is fully integrated with a digitally controlled PPU, providing the power and control for all necessary subsystems to operate the thruster.

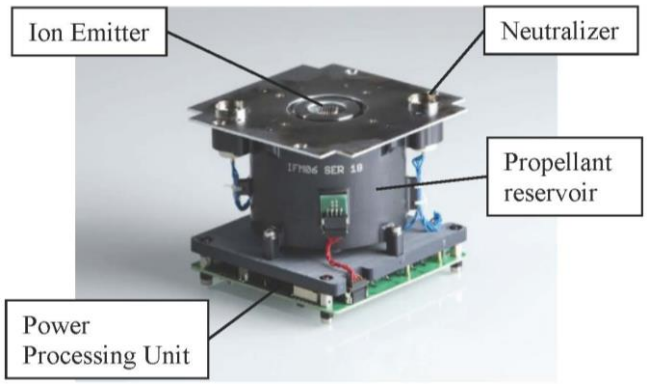

Figure 2. IFM Nano Thruster.

2.3. Emitter Selection: Emitter Impedance and Mass Efficiency

Figure 3 shows the operational envelope of an IFM Nano Thruster with 35% mass efficiency evaluated at 4*mA* emission current, plotting the relationship between the thrust, specific impulse (*Isp*) and total system input power draw. *Isp* and thrust were computed by the thruster power processing unit used to operate the thruster during the campaign, provided to the user via telemetry. The thrust F and specific impulse *Isp* of a FEEP thruster can be approximated by Eqns. (1) and (2) respectively (Vasiljevich et al., 2008):

$$F = I \cdot \sqrt{2 \cdot V_e \cdot \frac{m}{q_e}} \cdot f \tag{1}$$

$$I_{sp} = \frac{1}{g_0} \cdot \sqrt{2 \cdot V_e \cdot \frac{q_e}{m}} \cdot \eta \cdot f \,, \tag{2}$$

in which I is the net emitted current, V_e is the emitter potential, q_e/m is the mass-to-charge ratio of a singly ionized indium ion, and g_0 is the standard acceleration due to gravity. The symbol f is a factor accounting for the beam spreading (f = 0.8) and η is the mass efficiency $\eta(I), with\, \eta_{4mA} = 35\% \pm 10\%$ of the emitter, which is a function of the emission current and depends on the microscopic emitter properties (Vasiljevich, 2010) and can be characterized for each emitter during acceptance testing. The beam factor or divergence f (Vasiljevich, 2005; Vasiljevich, 2008) was derived from spatial beam distribution measurements at FOTEC.

The mass efficiency, shown in Figure 4, is modeled according to a FEEP mass efficiency model (Tajmar, 2003; Tajmar, 2009; Jelem, 2016) based on statistical determination of mass efficiencies of emitters. During emitter production, the mass efficiency is measured for each emitter by weight measurements before and after a constant emission current firing period, according to Eqn. (3). By emitter selection during production, specific ranges of mass efficiency can be chosen for the final thrusters:

$$\eta_{4mA} = \frac{\Delta M}{\Delta I} \frac{q_e}{m} \,, \tag{3}$$

where ΔM is the propellant consumption and ΔI is the integrated current over the test duration. Due to uncertainties in the underlaying model, we assume an uncertainty of 10% for the mass efficiency.

The total input power includes the beam power with electrical losses, the heater to maintain the propellant in liquid state, and the heating power necessary to operate the neutralizer at an electron emission current matching the ion emission current. In the current version of the IFM Nano Thruster, the PPU is designed for a maximum input power of up to 40 *W*. The iso-power lines in Figure 3 indicate the operational points available for a given input power. In a spacecraft with 40 *W* available for propulsion, the

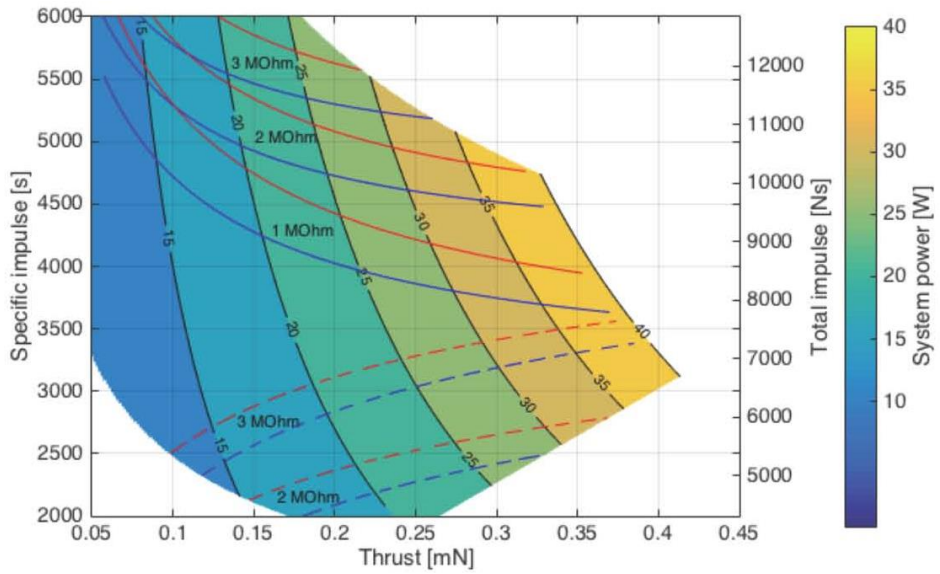

Figure 3. IFM Nano Thruster operational envelope with modelled emitter impedance, assuming 220g of propellant (assuming ~95% filling level). Startup discharge voltages are 6 kV (blue) and 7 kV (red).

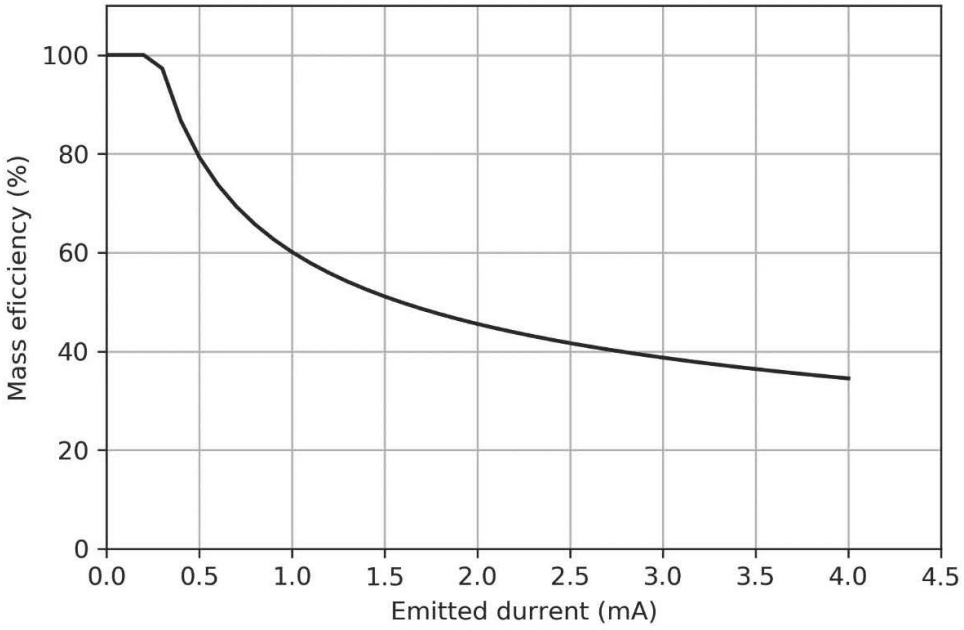

Figure 4. Current dependency of the mass efficiency.

IFM Nano Thruster depicted can, for example, be operated at a thrust of F~400 μ*N* with specific impulse of 3200 s for a maneuver where higher thrust is required. In a later stage of the mission in which lower thrust levels but high specific impulse is desired, the thruster could then be operated at *F*~200 μ*N* and an *Isp* of 4500 s at a reduced input power of ~25 *W*. Figure 3 also shows the maximum *Isp* constraint imposed by the current PPU in terms of maximum absolute emitter voltage. Note that this constraint is imposed by the PPU and is not a physical parameter of the ion emitter.

Based on the emitter impedance, that is the relation between applied discharge potential and emis-

sion current, a selection of emitters suitable for specific regions of the performance map can be performed. The impedance Z of an emitter is defined as:

$$V_D = V_0 + ZI\,, \tag{4}$$

with V_D the discharge voltage, V_0 the startup voltage, and I the emission current. Figure 4 shows the IFM Nano Thruster with PPU emitter voltage limit, with modelled emitter impedances. Given the high voltage limits of the IFM Nano Thruster PPU in terms of maximum emitter and extractor voltage, Figure 3 indicates the lower and upper operational bounds for a modelled emitter. For low impedance emitters of 1 *MΩ* as tested in this campaign, the lower specific impulse limit is below 2000 *s*, whereas the upper bound restricts to values between 3500 *s* at maximum thrust and increases up to 5500 *s* for lower thrust settings. Such emitters are therefore optimized for higher thrust operation at lower power draws. Higher impedance emitters on the other hand can be preferably used for mission scenarios that require high *Isp* operation. Regardless of emitter selection, a wide throttling range of ~3000 *s* is available, primarily limited by current IFM Nano Thruster PPU limits.

The current version of the IFM Nano Thruster features a propellant reservoir of up to 230 *g* of indium propellant, which results in total impulse ranging from 5 to >10 *kNs*, depending on chosen operation setpoint.

However, small customization allows for different propellant reservoir sizes. Figure 5 shows a design study regarding the impact of propellant reservoir size changes on the volume requirement of the IFM Nano Thruster. In the reduced size configuration shown, the total impulse that can be achieved reduces to approximately 300 to 700 *Ns*. While specific impulse and thrust values remain comparable with the standard IFM Nano Thruster, slight increase in efficiency is found due to decreasing thermal losses of the hot propellant reservoir. The decreased propellant loading results in a significant decrease of necessary preheating time and heating power required for propellant liquification and to reach the operational temperature. It should be noted that while even smaller packages are conceivable for reduced propellant loading, the configuration shown in Figure 5 is not optimized for miniaturization, but to maintain the heritage of the IFM Nano Thruster by decreasing the reservoir size without impacting any other design features, and without changing any of the functional systems of the thruster regarding propellant distribution and ion emission.

3. Test Campaign and Setup Description

Two IFM Nano Thrusters were used in this test campaign, to perform direct thrust measurements and comparison to the established thrust models, and to perform full performance envelope mapping. In these envelope mapping tests, the thrusters were operated at different operation points covering the entire thruster range in terms of thrust and specific impulse. In addition, specific operation modes including the

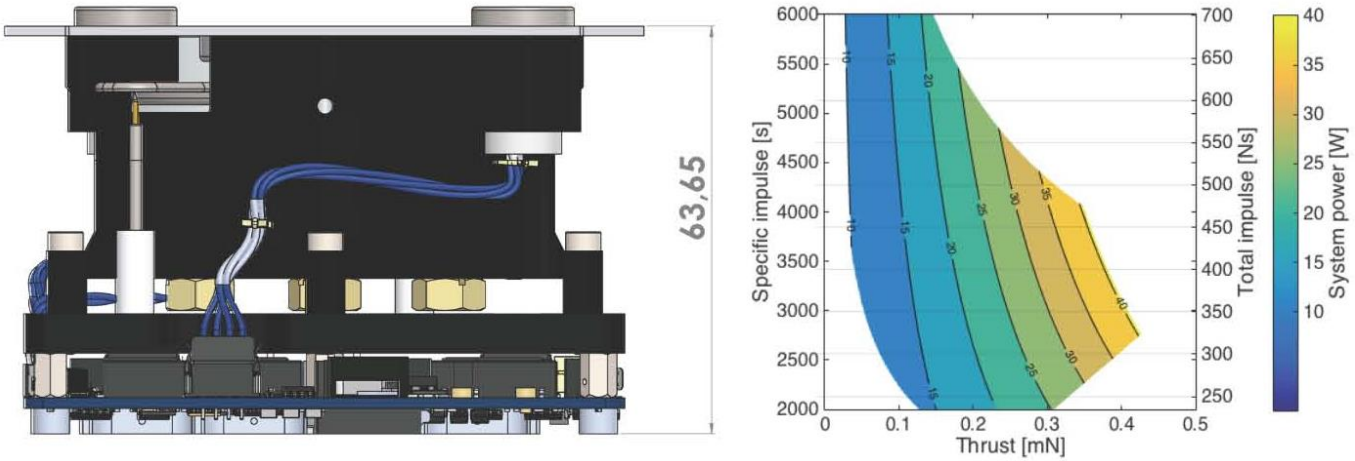

Figure 5. IFM Nano Thruster reduced size option and resulting performance map with total impulse values.

ability to throttle specific impulse for constant thrust, are presented. The *Isp* computation is done via a model based on empirical values according to Eqn. (2) and is therefore dependent on the mass efficiency model described in Sec. 2.3.

3.1. ESA ESTEC Thrust Stand Facility and Measurement Uncertainty

The IFM Nano Thruster direct thrust measurement campaign was performed within the GALILEO vacuum facility of the ESA Propulsion Laboratory (EPL) at ESA-ESTEC (Dannenmayer, 2016). Two fully integrated IFM Nano Thrusters, designated IFM06.25 and IFM06.26, were used in this test campaign. The thrusters were mounted on a Mettler-Toledo thrust balance XP2004S. The temperature inside the chamber was recorded with type K thermocouples placed on the passive cooling system, the thrust balance itself, the chamber wall, and on the aluminum block under the thruster, which was acting as passive heat dissipation system. Two different computers and TTi low-voltage power supplies were used for operations of thruster and thrust balance re spectively. The IFM Nano Thruster was controlled via an USB adapter using the RS-422 communication protocol. Meanwhile, the thrust balance was operated via RS-232 protocol. The force actuator placed between the IFM Nano Thruster mounting and the thrust balance used KEITHLEY 2000 and 2040 power supplies respectively, which were controlled by an RS-232 protocol via a laboratory computer. The XP2004S thrust balance has a resolution of 1 μN (i.e., 0.1 *mg*) with a maximum weight load of 2.3 *kg*.

A passive cooling system to remove heat from the thruster PPU was used, which comprised a heat sink coupled to a radiative surface. The thermal control was only used to remove heat generated from the power processing unit as no thermal control of the thruster head, or propellant reservoir was required.

Preliminary calibrations were performed on the thrust balance using several calibrated masses from 0 to 1*g* that were placed on the balance to calibrate the balance to the norm masses. A second calibration procedure validated the linearity and repeatability of the balance by exciting the force actuator (FA) with a current ranging from 0 to 2.4 *mA* in steps of 0.25 *mA*. These steps were repeated three times for each thruster installed on the balance. The uncertainties resulting from these calibration procedures are summarized in Table 1.

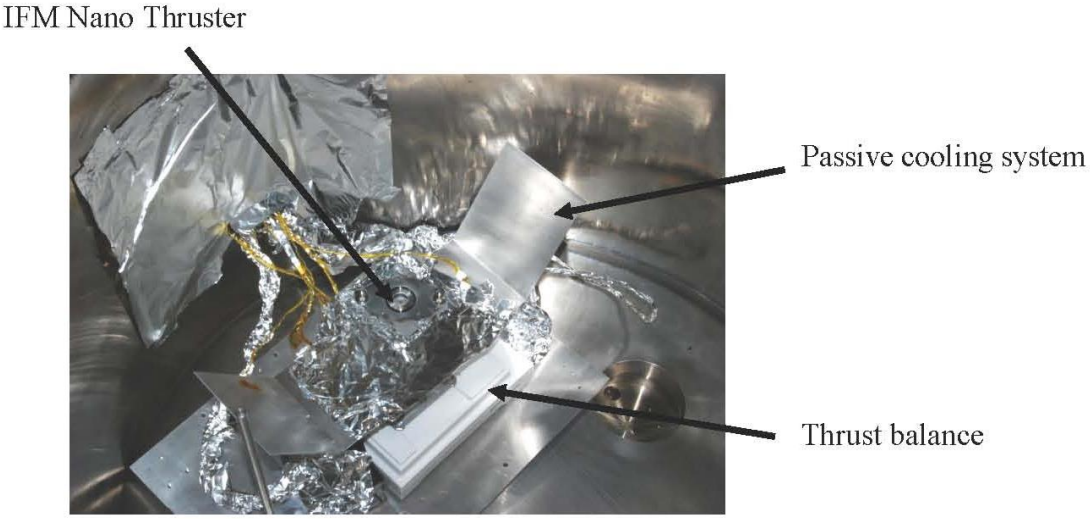

Figure 6. IFM Nano Thruster mounted to the EPL thrust balance.

Table 1. Estimated Standard Uncertainties of Mounted Thrusters on the Balance

Round	FA scale [μN] (Reference)	IFM06.26 [μN]	IFM06.25 [μN]
Standard uncertainties (u)	1.29	4.81	0.95

One can notice that for the set-up with the IFM06.26 installed, u is close to five times the uncertainty of the reference set-up case, while the calibration standard uncertainty found for IFM06.25 is less than 1%. An additional drift test was performed in order to assess the impact of the pumping system on the set-up. In this step, three calibration runs were performed for each thruster, with resulting uncertainties given in Table 2, showing the negligible influence from the pumping system on the total uncertainty budget.

Finally, a thermal drift of 1 *mN*/1000s was recorded during thrust measurements at 280µ*N* for 15 min. This shows that the drift is higher than the thrust aimed to be measured. It is therefore evident that it is not possible to measure the average thrust out of a constant firing mode in this setup. Therefore, facilitated by the benign on/off behavior of FEEP ion emitters, which do not exhibit start-up delays or current overshoots, thrust measurements were performed by evaluating the difference between firing and idle thruster operation over 1s on/off step times. A firing procedure with stepwise 50s on-off cycling was used and thrust measurements reported were determined by the difference of thrust measured between firing and idle mode. Therefore, the time in which thermal drift can occur is significantly reduced, and the corre sponding contribution to the measurement uncertainty reduces to 0.58µ*N*. Although the working principle of the thrust balance would have allowed for in-situ *Isp* measurements, this was prevented by the thermal drift due to heat dissipation in the passive thermal setup.

3.2. Measurement Accuracy

Since the thrust and the specific impulse are computed by the processing power unit according to Eqns. (1) and (2), they rely on parameters measured by the PPU. Both the accelerating voltage and the emitted current have a precision reading of 1%, with additional measurement noise during operation. The worst-case scenario for deviation from the average value is found as 0.4% for the accelerating voltage, 6.4% for the emitted current in thrust control mode while only 0.5% when this parameter is directly controlled. Using quadrature summation according to Eqn. (5), the resulting standard uncertainties of these three parameters are summarized in Table 3.

The parameter uncertainties for thrust and specific impulse are calculated according to error propagation using Eqns. (6) and (7).

$$u = \sqrt{\sum_{i=1}^{n} u_i^2}\,, u_{95\%} = 2u \tag{5}$$

$$\frac{u(T)}{T} = \sqrt{\left(\frac{u(V_e)}{V_e}\right)^2 + \left(\frac{u(I)}{I}\right)^2} \tag{6}$$

$$\frac{u(I_{sp})}{I_{sp}} = \sqrt{\left(\frac{u(V_e)}{V_e}\right)^2 + \left(\frac{u(\eta)}{\eta}\right)^2} \tag{7}$$

An uncertainty budget was performed for the measured thrust. Uncertainties induced by the installation are summarized in Table 1. The influence from the pumping system was assessed and found negligible (Table 2) and was therefore neglected. The thermal drift for firing steps of duration 1s, the balance precision, the reading of the commanded thrust by the PPU (1%) as well as uncertainty of calculated thrust and specific impulse according to error propagation and the signal noise (0.5 %) were evaluated. Table 4 provides a summary of the derived uncertainties as well as the final standard uncertainties with a confidence level of 95% (k = 2). The final uncertainty was obtained with a quadrature summation equation as per Eqn. (5).

Table 2. Estimated Standard Uncertainties of Drift Caused by the Pumping System

Round	IFM06.26 drift [µN]	IFM06.26 drift [µN]
Standard uncertainties (u)	0.004	0.0007

Table 3. Estimated Standard Uncertainties of the PPU Readings Parameters

Parameters	Estimated standard uncertainty (%)
Acceleration voltage	± 1.01
Emitted current	± 6.47
Mass efficiency	± 10

4. Direct Thrust Measurements and Comparison to Onboard Thrust Model

4.1. V-I Mapping

Before conducting direct thrust measurements, the emission characteristics of each thruster was de termined by measuring the emitter impedance at different extractor voltages. This allowed comparison with the impedances measured during thruster acceptance testing at ENPULSION, verifying the nominal operation of both thrusters. For these measurements, onboard telemetry was used to determine the required emitter voltage to achieve certain commanded emission currents. V-I curves based on that data are shown in Figure 7.

4.2. Direct Thrust Measurements at Constant Extractor Voltage

Figure 8 shows directly measured thrust and *Isp* calculated by the PPU and transmitted via telemetry as a function of beam power for the two thrusters tested, using a constant extractor. Figure 9 shows the same data as a function of the total system input power including propellant heating and neutralizers. To simulate a worst-case scenario, the neutralizers were operated at maximum power during these tests.

Table 4. Estimated and Final Standard Uncertainties of the Measured Thrust with a Confidence Level of 95%

Parameters	IFM06.25 standard uncertainties (μN)	IFM06.26 standard uncertainties (μN)
Installation	± 0.95	± 4.81
Thermal drift	± 0.58	± 0.58
Balance precision	± 0.58	± 0.58
The computed thrust (from error propagation, PPU readings, oscillation)[1]	$\pm[12.26, 13.73, 15.04, 15.78, 17.11, 18.32, 19.45]$	$\pm[12.26, 13.73, 15.04, 15.78, 17.11, 18.32, 19.45]$
Final uncertainty [1]	$\pm[3.9, 4.9, 5.8, 6.3, 7.1, 7.8, 8.5]$	$\pm[6.1, 6.9, 7.5, 7.9, 8.6, 9.2, 9.7]$
Final uncertainty with a confidence level of 95%)[1]	$\pm[7.8, 9.9, 11.7, 12.7, 14.3, 15.7, 17.0]$	$\pm[12.2, 13.7, 15.0, 15.8, 17.1, 18.3, 19.5]$

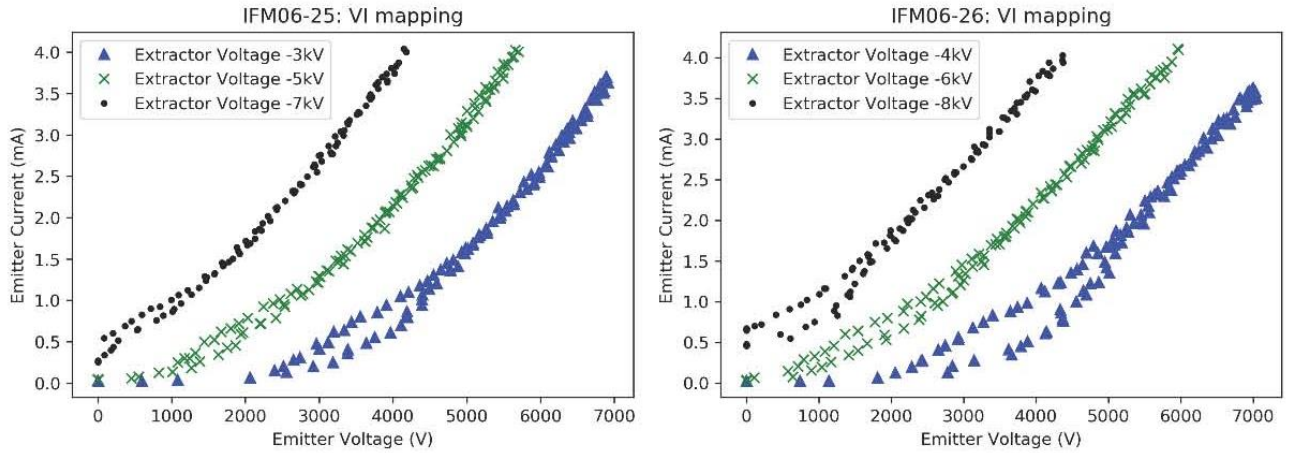

Figure 7. V-I mapping of two IFM Nano Thrusters on EPL thrust balance.

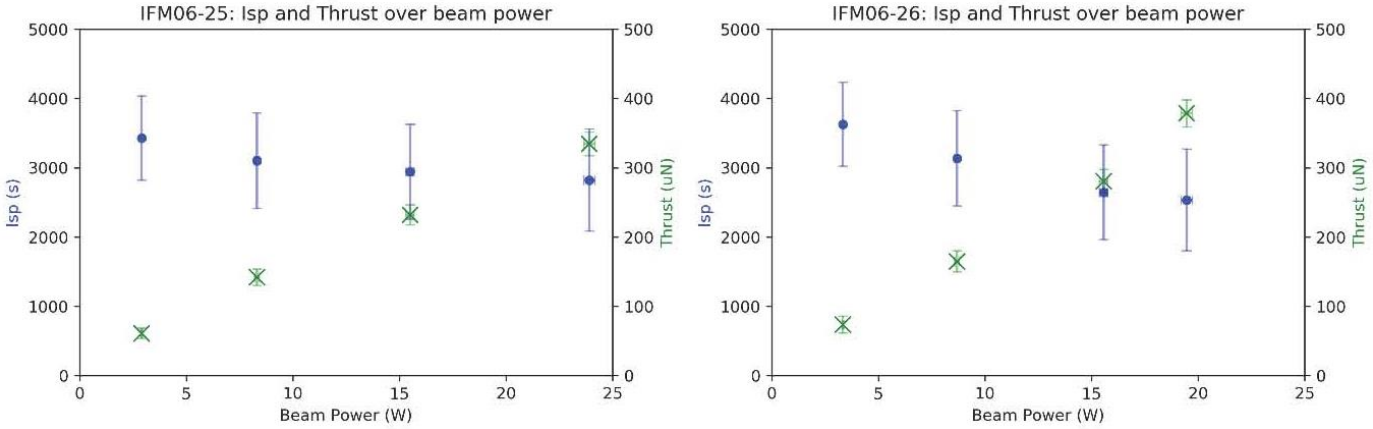

Figure 8. Directly measured thrust and calculated specific impulse as a function of input power without neutralization of two IFM Nano Thruster.

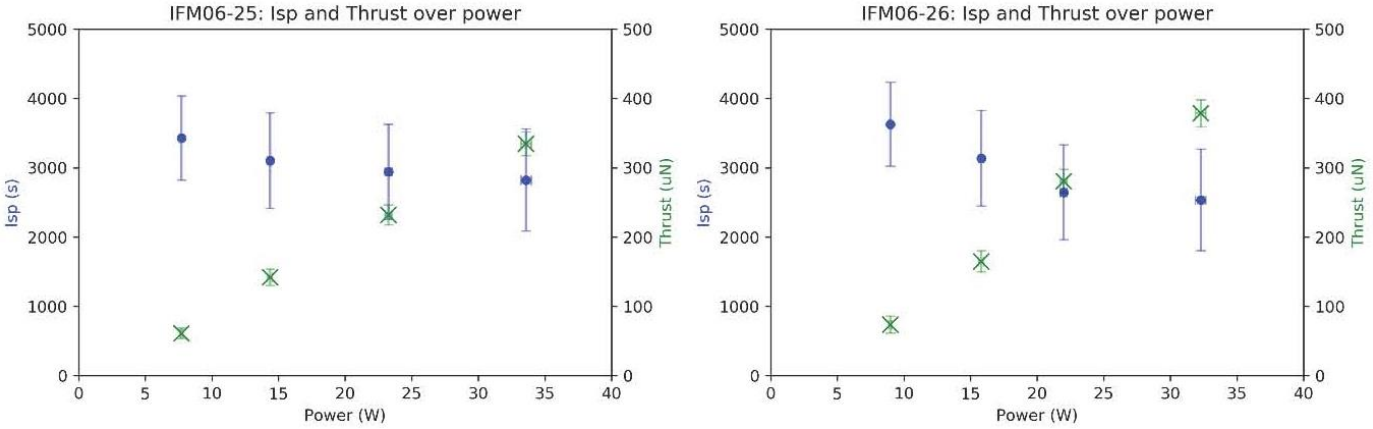

Figure 9. Measured thrust as a function of input power including neutralization of two IFM Nano Thruster.

4.3. Throttling of Specific Impulse at Constant Thrust

A feature of the FEEP technology is the ability to throttle in specific impulse over wide ranges at approximately constant thrust. In the test campaign, tests were performed commanding constant thrust, while throttling over different specific impulse val ues. In this test, 300–350 µ*N* were commanded, and extractor voltage was varied to achieve different specific impulse levels. Note that at 350 µ*N*, which is close to the maximum thrust operation point, the *Isp* envelope over which throttling can be performed is narrower than at lower thrust levels. Figure 10 shows the resulting specific impulse achieved when controlling the thruster to approximately constant thrust levels around 300–350 µ*N*.

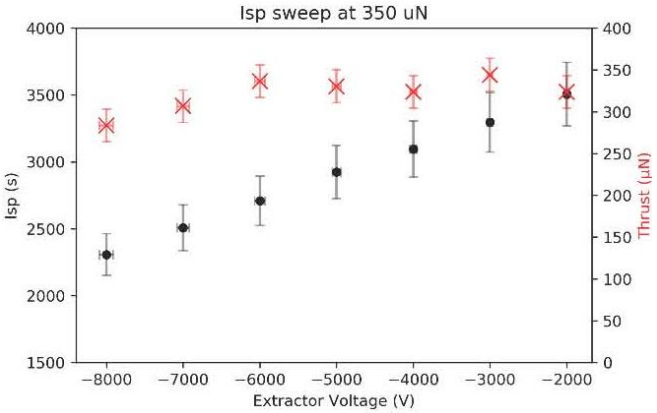

Figure 10. Specific impulse derived from measured data of an IFM Nano Thruster throttled over different specific impulse values while operated at constant thrust.

4.4. Comparison of Direct Thrust Measurements with Modelled Thrust Provided by Onboard Telemetry

Figure 11 presents a comparison of the experimentally determined thrust values with the thrust modelled using Eqn. (1), which has been directly calculated by the IFM Nano Thruster PPU and is part of the telemetry data.

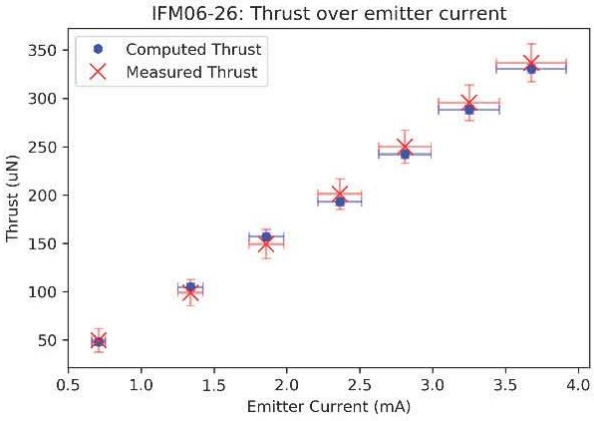

Figure 11. Measured thrust vs modeled thrust (from telemetry) as a function of emission current of an IFM Nano Thruster.

5. Experimental Performance Envelope Mapping

5.1. Experimental Performance Envelope Mapping: Total Input Power

The two thrusters tested in this campaign were equipped with emitters optimized for medium specific impulse and high-thrust operational point, that is, emitters with low onset voltage and low impedance. Such emitters allow for lower *Isp* operation.

For the evaluation of power draw, two cases were considered: beam power was calculated by the product of emitter voltage and current as measured by the thruster PPU, whereas total system input power was evaluated by the low voltage input bus voltage and current of the PPU, again measured by the thruster. The latter includes the PPU inefficiencies due to conversion, the power required to heat the propellant reservoir to the operational temperature and the neutralizer power consumption. The neutralizer power draw as a function of electron emission current is shown in Figure 12 for thruster IFM06.26. However, to simulate worst case conditions, the neutralizer was operated at maximum possible power draw of 6 *W* during the test campaign described below, which results in an overestimation of the required power consumption of approximately 2 *W*.

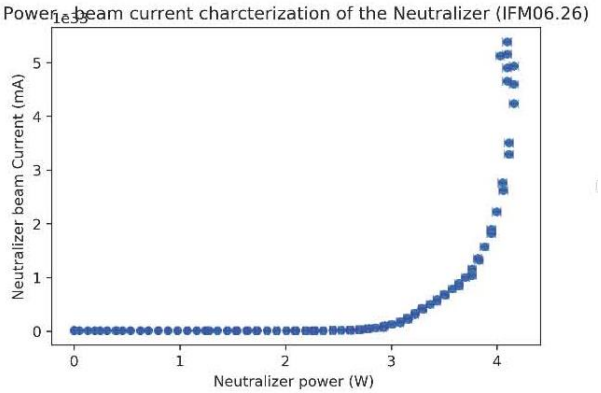

Figure 12. Neutralizer power consumption for a given beam current.

Figures 13 and 14 show the experimentally determined performance maps of thrusters IFM06.26 and IFM06.25 respectively, plotting the relationship thrust, specific impulse, and total system input power on the left-hand side and based on beam power on the right-hand side. Note that thrust and system power were measured directly, whereas specific impulse and beam power were determined by the PPU according to telemetry. Note also that uncertainties of data are not plotted for readability reasons. The total system input power includes power consumed by the heater to maintain the propellant at operational state as well as power required for neutralization. To simulate a worst-case scenario, the neutralizer was operated at maximum power of 6 *W* throughout the campaign, which is a significant overestimation when compared to Figure 12.

Figure 15 shows an overlay of experimental data for IFM06.26 and the theoretical performance model based on beam power (left) and total system input power (right). The two tested thrusters show impedance values of 1–1.2 $M\Omega$ and onset voltages of $V_0 \approx 6kV$. Due to the low impedance, the maximum specific impulse for these emitters is therefore limited as indicated by the blue line: max *Isp* values of ~4500

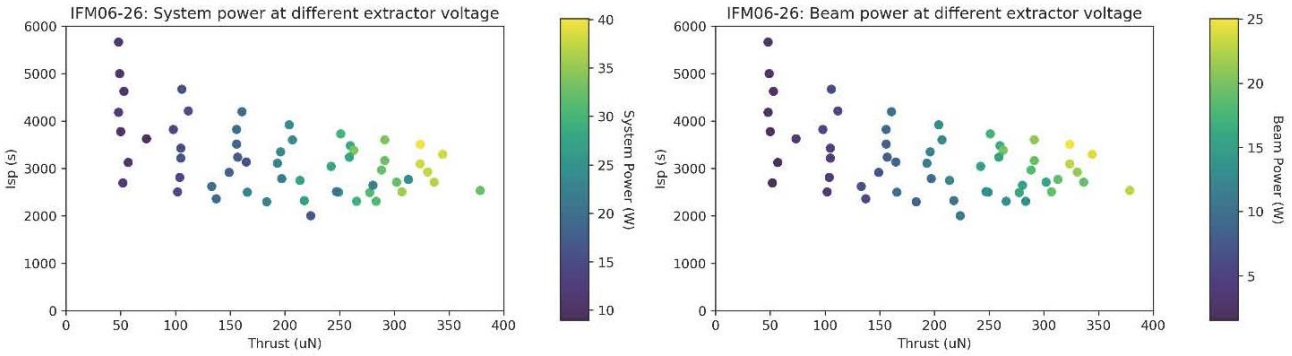

Figure 13. Performance map of IFM06-26 IFM Nano Thrusters based on total input power (neutralizer max power draw) (left) and beam power (right). Uncertainties according to Section 3.2 not shown for readability reasons.

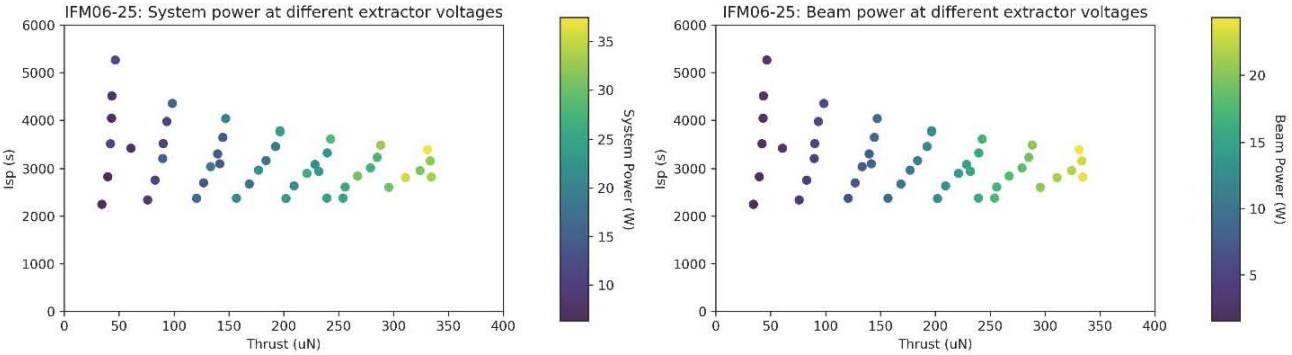

Figure 14. Performance map of IFM06-25 IFM Nano Thrusters based on total input power (neutralizer max power draw) (left) and beam power (right). Uncertainties according to Section 3.2 not shown for readability reasons.

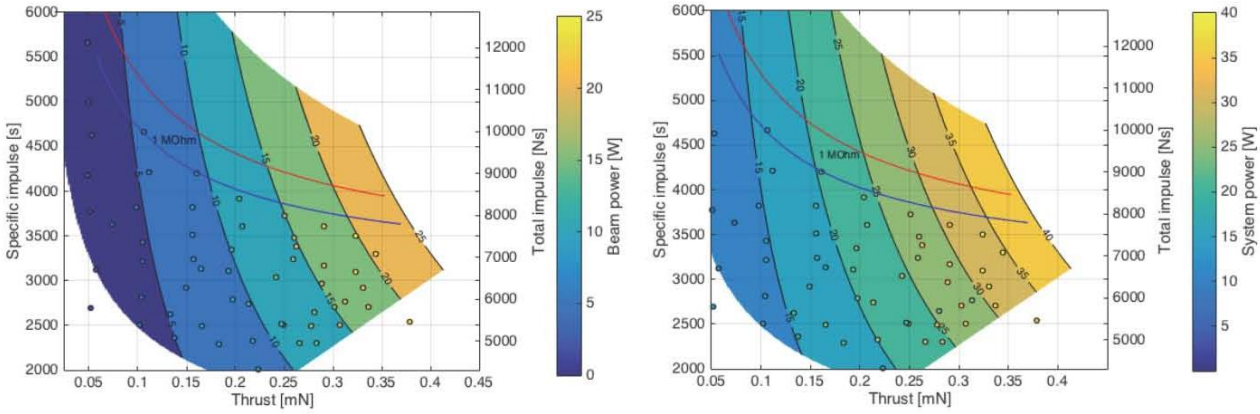

Figure 15. Comparison of tested thruster envelope (round markers), to modelled performance envelope matching the 6 kV, 1MΩ characteristics of IFM06.26. Left: Beam power, right: system power with neutralizer at max. power draw. Uncertainties according to Section 3.2 not shown for readability reasons.

s at 150 µ*N*, to ~3700 *s* at 350 µ*N*. For these emitter properties, the limit for minimum *Isp* is outside of the plotting region.

Figure 15 shows good agreement of the tested thrusters with the modelled performance envelope when considering the specific emitter characteristics of onset voltage and emitter impedance. As discussed above, neutralizer power draw was increased to maximum in the experimental campaign to study worst case conditions.

6. Conclusion

The IFM Nano Thruster is a Cubesat-sized liquid metal FEEP thruster that can provide high-specific-impulse propulsion to a wide variety of spacecraft. In the presented work, two IFM Nano Thrusters have been characterized in the propulsion laboratory at ESA ESTEC. Data presented include results from direct thrust measurement ranging from ~50 to ~380 μ*N* at thruster input power levels from 9 to 40 *W* including propellant heating and neutralization. A full performance mapping of the thruster is presented based on experimental thrust measurements, including the thrusters' ability to significantly vary specific impulse over a range of more than 3500 *s*. The presented results verify the thrust generated and show good correlation of the measured thrust level with the FEEP thrust models used in the IFM Nano Thruster telemetry.

References

Afrose, M. F., Masood, S. H., Nikzad, M. et al. (2014): Effects of Build Orientations on Tensile Properties of PLA Material Processed by FDM. *Adv. Materials Research*, Vol. 1044, pp. 31–34.

Dannenmayer, K., Bosch Boras, E., Gonzales del Amo, J. (2016): ESA Propulsion Laboratory at ESTEC, presented at the 5th Space Prop. Conf., Rome, Italy.

Fehringer, M., Ruedenauer, F., Steiger, W. (1997): Space-Proven Indium Liquid Metal Field Ion Emitters for Ion Microthruster Applications, presented at the 33rd AIAA/SAE/ASEE Jt. Prop. Conf. and Exhibit, Seattle, WA. Paper AIAA-1997-3057.

Jelem, D. (2016): Development of a Performance Model for a Field Emission Electric Propulsion System, Master's Thesis, FH, Wiener Neustadt, Austria.

Jelem, D., et al. (2017): Performance Mapping and Qualification of the IFM Nano Thruster FM for in Orbit Demonstration, presented at the 53rd AIAA/SAE/ASEE Jt. Prop. Conf., Atlanta, GA. Paper IEPC-2017-24.

Krejci, D. and Lozano, P. (2018): Space Propulsion Technology for Small Spacecraft, in *Proc. IEEE, Vol. 106, No. 3*, Mars, pp 362–378.

Krejci, D., et al. (2018): Demonstration of the IFM Nano FEEP Thruster in Low Earth Orbit, presented at the *4S Symposium*, Sorrento, Italy, May-June, p. 56.

Lemmer, K. (2017): Propulsion for Cubesats. *Acta Astronautica*, Vol. 134, pp. 231–243.

Mair, G. L. R. (1996): Electrohydrodynamic Instabilities and the Energy Spread of Ions Drawn from Liquid Metals. *J. Phys. D.: Appl. Phys.*, Vol. 29, pp. 2186–2192.

Reissner, A., et al. (2015): Testing and Modelling of the mN-FEEP Start-Up Performance, presented at the 34th Int. Electric Prop. Conf., Hyogo-Kobe, Japan. Paper IEPC-2015-123.

Seifert, B., et al. (2018): In-Orbit Demonstration of the Indium-FEEP IFM Nano Thruster, presented at the 6th Space Prop. Conf., Seville, Spain.

Selva, D. and Krejci, D. (2012): A Survey and Assessment of the Capabilities of CubeSats for Earth Observation. *Acta Astronautica*, Vol. 74, pp. 50–68.

Spangelo, S. and Longmier, B. (2015): Optimization of CubeSat System-Level Design and Propulsion Systems for Earth-Escape Missions. *J. of Spacecraft and Rockets*, Vol. 52 (4), pp. 1009–1020.

Tajmar, M. and Genovese, A. (2003): Experimental Validation of a Mass Efficiency Model for an Indium Liquid Metal Ion Source. *Appl. Phys. A* Vol. 76, 1003–1006.

Tajmar, M. (2005): Influence of Taylor Cone Size on Droplet Generation in an Indium Liquid Metal Ion Source. *Appl. Phys. A*, Vol. 81, pp. 1447–1450.

Tajmar, M., et al (2009): Liquid-Metal-Ion Source Development for Space Propulsion at ARC. *Ultramicroscopy*, Vol. 109, pp. 442–446.

Tajmar, M. (2009): Experimental Evaluation of the Critical Current in Indium LMIS. *J. of Phys. D: Appl. Phys.*, Vol. 42, 055506 (4pp).

Tajmar, M., Genovese, A., and Steiger, W. (2004): Indium Field Emission Electric Propulsion Microthruster Experimental Characterization. *J. of Prop. and Power*, Vol. 20 (2), pp. 211–218.

Tajmar, M., Vasiljevich, I., Grienauer, W. (2010): High Current Liquid Metal Ion Source Using Porous Tungsten Mutiemitters. *Ultramicroscopy*, Vol. 111, pp. 1–4.

Tajmar, M. (2002): Survey of FEEP Neutralizer Options, presented at the 38th AIAA/SAE/ASEE Jt. Prop. Conf., Indianapolis, IN. Paper AIAA 2002-4243.

Taylor, G. I. (1964): Disintegration of Water Drops in an Electric Field, *in Proc. of the Royal Society A, Vol. 280, No. 1382*, July, pp. 383–397.

Vasiljevich, I., et al. (2005): Development of a Focus Electrode for an Indium FEEP Thruster, presented at the 41st AIAA/SAE/ASEE Jt. Prop. Conf., Tucson, AZ. Paper AIAA 2005-4384.

Vasiljevich, I., et al (2008): Development of an Indium mN-FEEP Thruster, presented at the 44th AIAA/SAE/ASEE Jt. Prop. Conf., Hartford, CT. Paper AIAA 2008-4534.

Vasiljevic, I., et al. (2011): Consolidation of Milli-Newton FEEP Thruster Technology based on Porous Tungsten Multiemitters, presented at the 47th AIAA/SAE/ASEE Jt. Prop. Conf., San Diego, CA. Paper AIAA 2011-5592.

Vasiljevich, I (2010): Design, Development and Testing of a Highly Integrated and Up-Scalable FEEP-Multi Emitter Using Indium as Propellant, PhD thesis, TU, Vienna, Austria.